ISIJ International, Vol. 51 (2011), No. 3, pp. 365–374

Mathematical Modeling Study on Combined Side and Top Blowing AOD Refining Process of Stainless Steel

Ji-He WEI,[1)] Ying CAO,[1)] Hong-Li ZHU[1)] and He-Bing CHI[2)]

1) Department of Metallic Materials, College of Materials Science and Engineering, Shanghai University, Shanghai, 200072 P. R. China. 2) Stainless Steel Branch, Baoshan Iron & Steel Co., Ltd., Shanghai, 200431 P. R. China.

(*Received on July 7, 2010; accepted on December 6, 2010*)

Mathematical modeling of the combined side and top blowing AOD refining process of stainless steel has further been studied. A new model proposed is generally based on the analysis and assumptions made for the process in our previous investigation. Particularly, the heat transfer characteristics of the vessel are analyzed in terms of the two-dimensional transient heat-conduction problems of composite walls. The heat and mass balances of the system are more comprehensively and precisely performed. The model has been applied to 28 heats of 304-grade austenitic stainless steel refining in a 120 t AOD converter. The results present that the changes in the composition and temperature of the liquid steel with the time during the whole process can be accurately predicted using the model. The competitive oxidation among the elements in the steel during the oxidative refining with the relevant oxygen distribution ratios, and the competitive reduction of the oxides in the slag during the Ar agitating and reductive refining with the appropriate oxygen supply ratios can be well characterized and reasonably determined using the Gibbs free energies of the reactions. The critical carbon concentrations (after which the decarburization alters to be limited by the mass transfer of carbon in liquid steel) for the top, side and combined blowing of 304-grade steel in this work are in the ranges of 0.895 to 0.942, 0.078 to 0.224, 0.144 to 0.255 mass%, respectively. The effects of some factors on the refining result and the optimization of blowing technology have been considered from the model predictions. The model can provide a reliable basis and useful information for determining and optimizing the technology of this AOD process of stainless steel, and controlling the process in real time and on-line.

KEY WORDS: stainless steel; AOD refining; combined side and top blowing process; mathematical modeling.

1. Introduction

The argon–oxygen decarburization (AOD) process has been widely used and rapidly developed throughout the world due to its remarkable advantages, now being an integral part of the manufacturing route of stainless steel. Especially, in the recent years, taking high-carbon high-chromium hot metal as the main raw material with combined side and top blowing operation has been in quite extensive use, particularly in a large converter for decreasing the scrap and energy consumptions and the production cost. This is one of technological progresses of the process and has become a development tendency.

During the past several decades, simultaneously, many investigations on mathematical modeling for the process with horizontal side (traditional) blowing have been conducted. Numerous models have been developed to make its technological optimization and computer control,[1–11)] which have been reviewed by Wei and Zhu.[12)] Also, considering the strong and weak points of those models, they studied further this process, developing a more reasonable and reliable mathematical model for the decarburization during the process.[12)] In the model, the influences of the various operations, non-isothermal conditions and others were all taken into account. The model was applied to the steelmaking of 18Cr9Ni-grade in an 18 t AOD vessel with two side tuyeres, obtaining good results and useful information.[13)]

The situations in a combined side and top blowing AOD refining process are much more complicate than those in a simple side blowing one as a result of introducing an oxygen top blowing jet for intensifying and accelerating decarburization. Thus, it will be more difficult to mathematically model this type process. Our group[14–16)] first investigated preliminarily mathematical modeling of the complicate process. Noticing the related physical and chemical characteristics including the thermodynamic and kinetic properties, considering the heat and mass balances of the system and the effects of the various operations, a mathematical model for the whole refining process of stainless steel, including the oxidizing and reducing, was proposed. The model was used to simulate and estimate the designed refining of austenitic stainless steel in a 120 t AOD converter with seven side tuyeres and one top lance. Quite good results were obtained, providing useful information for putting the converter into operation. However, the converter was not completed when carrying out the investigation, thus having no practical example of production and lacking many key data. In this case, the related initial and boundary conditions, the physical properties of the refractory materials and others used for simulating and estimating could not be more properly determined, and also had considerable deviations from the existing practice. Moreover, the heat

losses of the parts of the vessel were approximately evaluated only based on the one-dimensional transient heat-conduction problems, like those done in mathematical modeling of simple side blowing AOD process.[12,13] In this case, the heat balance made for the system was not accurate enough, difficult to consider properly the non-isothermal conditions of the process. Therefore, a new mathematical model has been proposed and developed. In this new model, particularly, the heat transfer analysis of the vessel has been improved. In order to examine its applicability to practice, it has been applied to 28 heats of 304-grade austenitic stainless steel refining in a 120 t AOD converter. Also, the influences of the related factors on the refining result and the optimization of the blowing technology have been considered on the basis of the model predictions.

2. Mathematical Model

2.1. Rate Equations of the Refining Periods[14,16–18]

The oxygen top blowing operation does not change the numbers of substances and independent components in the system. Thus, it cannot alter the refining reaction schemes, which would be entirely the same as those in a simple side blowing. If the oxidation losses of the elements dissolved in the steel other than C, Cr, Si, and Mn are not considered, the two sets of independent reaction equilibria in the system, which are respectively corresponding to the indirect oxidation of the four elements in the steel and the direct reduction of the oxides in the slag by the carbon in the steel, can be generated from the direct oxidation reactions of the elements and Fe as the steel matrix by the blown oxygen.

From the physical and chemical characteristics, some initial assumptions were made for the combined blowing AOD process of stainless steel. On the basis of the assumptions, the average oxidation rates of the four elements in the steel at high carbon contents, the overall decarburization rates resulted from the top and side blowing oxygen at low carbon concentrations can be obtained. Besides, the average decarburization rates in the simple side blowing after finishing oxygen top blowing and in the Ar stirring and reduction refining after terminating oxygen supply can be derived, respectively. Correspondingly, the concentration change rates of Cr, Si and Mn in the steel can be obtained from the decarburization rate.

2.2. Temperature Field in Refractory Lining

The bath is always in different non-isothermal conditions during the whole refining process. Changing uninterruptedly in the bath temperature directly influences the equlibria and rates of the refining reactions, thus affecting progressing of the process. Physical modeling of this process[17,19,20] showed that by driving of multiple gas side blowing streams and impinging of gas top blowing jet, the liquid in the whole bath is in vigorous agitation and circulatory motion during the process. Relevantly, strong convection heat transfer would occur in the bath. On the other hand, there exist the heat sources arisen from the oxidation reactions of elements and the post-combustion of CO escaping from the bath in the system. Simultaneously, the heat of the system can be lost by conduction and adsorption of the lining and shell during the rising-temperature process of the bath; by radiation; by the operations of sampling, measuring the temperature, and adding slagging and metallic materials; and by other factors.

As mentioned above, in the preliminary investigation,[14–16] the heat transfer of the vessel was approximately dealt with in terms of the one-dimensional transient heat-conduction of different multilayer plates. The results obtained in this way would have larger deviations from the realities. In order to enhance the precision of mathematical modeling, the relevant heat transfer characteristics have been analyzed in terms of the two-dimensional transient heat-conduction of different composite multilayer walls in this study. The vessel is divided into four parts: the bottom, the lower (the position below the slag line), the upper (the location non-contacted with the melts), and the top. For the temperature profiles in each part of the lining with the shell, the following equation can be held:

$$\rho_{\mathrm{ref}} c_{\mathrm{p,ref}} \frac{\partial T_{\mathrm{ref}}}{\partial t} = \frac{\partial}{\partial x}\left(k_{\mathrm{ref}} \frac{\partial T_{\mathrm{ref}}}{\partial x} \right) + \frac{\partial}{\partial y}\left(k_{\mathrm{ref}} \frac{\partial T_{\mathrm{ref}}}{\partial y} \right) + S_{\phi} \quad \text{.....(1)}$$

In the practical process, the heat exchange behaviors of the vessel with the molten steel and its surroundings are considerably complicate; the appropriate boundary conditions should be separately treated. In this work, a third kind boundary condition is taken for the outer interface of the vessel. The relevant heat transfer coefficients by convection and radiation are converted into a combined one. For the lower and bottom of the vessel, the first kind boundary conditions are all used. For the upper and top regions of the vessel over the bath surface, also, the third kind boundary conditions are similarly taken. Their heat transfer coefficients by convection and radiation are converted into a combined one, respectively. Thus, corresponding to Eq. (1), the initial conditions are:

for molten steel,

$$T_{\mathrm{m}} = T_0 \quad \text{.....(2)}$$

for the top of the vessel,

$$T_{\mathrm{ref}}(x, y, 0) = T_{\mathrm{ref_{t0}}} \quad \text{.....(3)}$$

for the upper of the vessel,

$$T_{\mathrm{ref}}(x, y, 0) = T_{\mathrm{ref_{u10}}}, \quad T_{\mathrm{ref}}(x, y, 0) = T_{\mathrm{ref_{u20}}} \quad \text{.....(4)}$$

for the lower of the vessel,

$$T_{\mathrm{ref}}(x, y, 0) = T_{\mathrm{ref_{l10}}}, \quad T_{\mathrm{ref}}(x, y, 0) = T_{\mathrm{ref_{l20}}} \quad \text{.....(5)}$$

for the bottom of the vessel,

$$T_{\mathrm{ref}}(x, y, 0) = T_{\mathrm{ref_{b10}}}, \quad T_{\mathrm{ref}}(x, y, 0) = T_{\mathrm{ref_{b20}}} \quad \text{.....(6)}$$

The boundary conditions are:

for the bottom and lower of the vessel,

$$T_{\mathrm{ref}}(x, y, t) = T_{\mathrm{ref_{m}}} \quad \text{.....(7)}$$

for the upper of the vessel,

$$-k_{\mathrm{ref}} \frac{\partial T_{\mathrm{ref}}}{\partial x} = a_{\mathrm{gru}}(T_{\mathrm{ref}} - T_{\mathrm{g}}) \quad \text{.....(8)}$$

for the top of the vessel,

$$-k_{\mathrm{ref}} \frac{\partial T_{\mathrm{ref}}}{\partial x} = a_{\mathrm{grt}}(T_{\mathrm{ref}} - T_{\mathrm{g}}) \quad \text{.....(9)}$$

for the outer surface of the shell,

$$-k_{\mathrm{ref}}\frac{\partial T_{\mathrm{ref}}}{\partial x}=a_{\mathrm{gro}}(T_{\mathrm{ref}}-T_{\mathrm{f}}) \quad \text{.....(10)}$$

where ρ_{ref} and $c_{\mathrm{p,ref}}$ are the density ($\mathrm{g\cdot cm^{-3}}$) and specific heat of lining ($\mathrm{J\cdot g^{-1}\cdot K^{-1}}$), respectively; T_{ref}, T_{m}, T_{g} and T_{f} are, respectively, the temperatures of lining, molten steel, gas and surroundings, K; k_{ref} is the heat conductivity of lining with vessel shell, $\mathrm{J\cdot cm^{-1}\cdot s^{-1}\cdot K^{-1}}$; S_{ϕ} is the source term, which is related with all the generation and loss terms of heat for each lining part in the refining process, dependent on the heat balance of the system[14]; a_{gru}, a_{grt}, and a_{gro} are the combined heat transfer coefficients of exhaust gas/upper lining, exhaust gas/top lining, and vessel shell/air interfaces, separately, $\mathrm{J\cdot cm^{-2}\cdot s^{-1}\cdot K^{-1}}$. In the subscripts of T_{ref}, t, u, l, b and m denote the top, upper, lower, bottom of the vessel, and the lining/molten steel interface, respectively; 1, 2 and 0 correspond to the upper and lower sections of the relevant parts, and the initial state, separately. The value ranges of x and y in Eqs. (3)–(10) are dependent on the real system. The temperature profiles in the lining with the shell can be obtained by solving Eq. (1) at the conditions given above, thus providing the necessary and reliable information and a basis for the heat balance of the system.

2.3. Heat Balance of the System and Rising Rate of the Bath Temperature

For the system, the heat balance equation can be achieved by considering all the heat in and out as well as the accumulation. Further, the relevant rising rate of the bath temperature can be obtained from the equation.[14] In the equations of the heat balance and rising rate, the overall heat loss of the system includes the heat dissipations of the vessel by conduction and radiation, by all the operations and some uncertain reasons during the refining process. The total heat absorbed by the lining of the vessel in bath temperature rising is equal to $W_{\mathrm{ref}}\,c_{\mathrm{p,ref}}\,\Delta T_{\mathrm{ref}}$ (being the sum of the heat absorptions of its four parts), here W_{ref} is the lining mass, g. In this work, the bottom, lower and upper, and top of the lining with the shell were referred to as a multilayer plate, composite cylindrical and conical frustum walls, respectively. The heat dissipations of the vessel by conduction and radiation, and the total heat absorbed by the lining were determined from the obtained temperature profiles in the four parts, separately.

2.4. Initial and Boundary Conditions

Besides Eqs. (2)–(10), the initial and boundary conditions involved in the model also include the initial masses of liquid steel and slag, the initial temperature and composition; the flow rates of oxygen and inert gas (N_2 or Ar) and their initial temperatures, the temperature of exhaust gas, the outer wall temperatures of the locations of the vessel, the amounts of addition agents and their temperatures, the temperature of lining, and so on. All of these were determined in practices.

3. Determination of Various Parameters

In this work, the previous calculation[12,13] was taken to determine the distribution ratios (x_{i}) of the blown oxygen among the elements dissolved in the steel and the "oxygen supply ratios" (x_{io})[14–16] of the oxides in the slag. Thus, the ratios are proportional to the Gibbs free energies of the oxidation and reduction reactions at the interfaces. Additionally, the activity coefficients of the components in the molten steel and slag, the equilibrium constants and standard Gibbs free energies of the reactions, the mass transfer coefficient of carbon in molten steel, the reaction interface areas in the top, side blowing and reductive refining, the oxidation enthalpies of the elements and other parameters were determined, based on our previous studies.[12,13,21–26] The values of heat conductivities of the refractory materials and shell (steel plate), the densities and specific heats of the related substances were taken from the practice. The combined heat transfer coefficients correlated with the parts of the vessel were determined by reference to the results given in Ref. 27).

The values of the oxygen utilization ratios in the blowing process used in the preliminary investigation were utilized. Accounting for the existing results[28] and the flow and mixing characteristics in an AOD bath with combined side and top blowing,[17,19,20,29] the relevant melting times of the addition agents, *i.e.* the time lapse values of their cooling effects, were determined in the light of the respective amounts and bath temperatures at the time of addition.

4. Numerical Solution

Based on the commercial code of PHOENICS, the related computer program has been worked out for solving the model. According to the program, whether there is the oxygen blowing operation or not is first judged before starting computation. If the process is at the oxidative refining period, the corresponding distribution ratios of blown oxygen are determined from the calculated Gibbs free energies of the oxidative reactions of the elements in the molten steel. Further, the decarburization rates controlled by the oxygen flow rate (dC_1/dt) and depended on the mass transfer of carbon in the molten steel (dC_2/dt) are calculated, respectively. Comparing these two rates, if $|dC_1/dt| < |dC_2/dt|$, the oxidation rates of the other elements are achieved with $|dC_1/dt|$. Otherwise, the appropriate oxygen amount consumed for decarburization is attained using $|dC_2/dt|$, and the oxidation rates of chromium, silicon, and manganese are computed using the remaining oxygen and the oxygen distribution ratios reached from the Gibbs free energies of their oxidation reactions. Then, the temperature fields of the parts of the lining are solved. The rising rate of the bath temperature is computed from the obtained temperature profiles and relevant heat losses of the parts as well as the heat balance of the system. The composition and temperature of the liquid steel at the next step are obtained by numerical integrating. The temperature fields of the lining are thereafter recalculated. The both mutually influence and alternately change. For solving of the temperature fields of the lining, the governing Eq. (1) and its fixed conditions (Eqs. (2)–(10)) are discretized using a control volume method, and the grid division of all computational domain is taken to be 20×128. The concentrations of the oxides in the slag can be determined from the mass balance of the system. For the Cr reduction period, the Gibbs free energies of the reduction reactions of the oxides are first evaluated. The oxygen supply ratios of the oxides in the slag and (dC_2/dt) are then calculated to obtain their reduction rates. Finally, the rising rate of the bath temperature and the concentrations of components in the molten steel and slag are computed in terms of the same steps and procedures. Since

FeO is regarded as an intermediate product of the oxygen blowing, its influence on the mass and heat balances in the oxidative refining can be ignored. The outputs of the model are the changes in the composition, temperature and amounts of the molten steel and slag melt, distribution ratios of oxygen among the elements and oxygen supply ratios of the oxides, decarburization rate, and temperature profile in the lining with the refining time.

5. Analysis and Discussion of Results

5.1. Verification of the Model

Five out of 28 heats 304-grade stainless steel refining in a 120 t AOD converter and the relevant operations are presented in **Tables 1** to **3**. In the practical production, the initial carbon contents of molten steel for all heats were lower than 4.2 mass%, and the initial concentrations of Si were all ≤0.35 mass%. The gas top and side blowing rates in the main decarburization period and the gas side blowing rates in periods 1 to 3 of the dynamic decarburization and reduction period were (110–140) O_2, $O_2:N_2=110:30$, 60 : 60, 40 : 80, 30 : (80–110), and (70–110) Ar Nm^3/min, respectively.

The carbon and chromium concentrations, bath temperatures at the endpoints of main decarburization and reduction periods of 28 heats predicted by the model are given in **Table 4** in comparison to those determined. The maximum absolute deviations of the predicted carbon and chromium concentrations and bath temperatures at the endpoints of main decarburization periods by the model from the determined values are 0.010, 0.647 mass% and 16 K, respectively. The absolute values of the relative average deviations correspond to 1.20, 0.69 and 0.12%, respectively. At the endpoints of reduction, those are 0.0002, 0.263 mass%, 15 K and 0.13, 0.57, 0.13%, separately. These fully demonstrate that the new model can more accurately predict the composition and temperatures of the bath at the endpoints of blowing periods than that proposed previously.[14–16] Therefore, its reasonability and reliability are well verified.

5.2. Changes in Composition and Temperature of Liquid Steel

The changes in the composition of liquid steel and bath temperature during the whole refining process (for heat 490) are presented in **Fig. 1**. This heat is the case of higher initial carbon (3.32 mass%). The figures denote, separately: 1, starting oxygen blowing; 2, adding active lime; 3, adding Fe–40Ni; 4, adding high-carbon Fe–Cr; 5, adding scrap or crop ends; 6, adding low-carbon Fe–Mn; 7, adding Fe–Si; 8, adding metallic Ni; 9, endpoint of oxygen top blowing operation; 10, endpoint of period 1 of dynamic decarburization; 11, endpoint of period 2 of dynamic decarburization;

Table 1. Related initial data and total refining times of some heats for 304-grade stainless steel refining in a 120 t AOD converter.

Heat No.	Initial mass of steel, t	Initial temperature, K	Initial composition of molten steel, mass%				Total refining time, min
			C	Cr	Mn	Si	
385	121.2	1820	2.22	17.77	0.39	0.35	53.1
387	116.0	1800	2.00	16.72	0.52	0.25	54.5
462	115.8	1809	2.90	17.16	0.44	0.23	52.9
479	122.6	1878	2.76	18.88	0.94	0.20	56.2
490	109.4	1860	3.32	17.58	0.43	0.16	54.4

Table 2. Gases and their flow rates used for some heats during combined side and top blowing refining process of 304-grade stainless steel in a 120 t AOD converter.

Heat No.	Cumulative time, s	Oxidative period of Si and Al			Main decarburization period			Period 1 of dynamic decarburization		Period 2 of dynamic decarburization		Period 3 of dynamic decarburization		Reduction period
		A	B	C	A	B	C	B	C	B	C	B	C	D
385	0	110	110	30										
	297				110	110	30							
	1226							60	60					
	1802									40	80			
	1989											30	110	
	2143													70
	3188													
387	0	110	110	30										
	297				110	110	30							
	1082							60	60					
	1587									40	80			
	1840											30	110	
	2169													80
	3268													
462	0	110	110	30										
	161				110	110	30							
	1230							60	60					
	1900									40	80			
	2152											30	110	
	2521													110
	3179													
479	0	110	110	30										
	296				140	110	30							
	1188							60	60					
	1783									40	80			
	2288											30	110	
	2601													100
	3374													
490	0	140	110	30										
	269				140	110	30							
	1256							60	60					
	1845									40	80			
	2082											40	80	
	2176													70
	3266													

*A—oxygen top blowing rate, B—oxygen side blowing rate, C—nitrogen side blowing rate, D—argon side blowing rate, Nm^3/min

Table 3. Addition agents and their amounts used for some heats during combined side and top blowing refining process of 304-grade stainless steel in a 120 t AOD converter.

Heat No.	Cumulative time, s	Amount of addition agent, kg									
		Active lime	High-carbon Fe-Cr	Low-carbon Fe-Mn	Scrap or crop ends	Fe-Ni	Metallic Ni	Fi-Si	Micro-carbon Fe-Cr	Dolomite	Fluorspar
385	0									1200	
	297	2500	3000		3000		2000				
	1226	2500	3000		9400		600				
	1802	3000									
	1989			770				2500			
	3188	1600									1300
387	0									1200	
	297	2500	5000		4000		2000				
	1082	2500	4800		4550		1650				
	1587	3000							700		
	1840			580				2640			
	3268	1500									1530
462	0	1002									
	161	2499	3010			5004					
	1230	2500	4006		5294	4688					
	1900	2496					214				
	2152			700				2439			
	3179	1398									1214
479	0										
	296	2501	2005			8059					
	1188	3000	2306		785	7936	1326				
	1783	2502			6485				890		
	2288			95				2444			
	3374	1399									1429
490	0									987	
	269	2501	3004			9004					
	1256	2499	5306		8006						
	1845	3000			4993		202		1343		
	2082			728				2594			
	3266	1801									1317

Table 4. Some model predictions and plant data for all the 28 heats.

Heat No.	Endpoint of main decarburization						Endpoint of reduction period					
	[C], mass%		[Cr], mass%		T, K		[C], mass%		[Cr], mass%		T, K	
	Predicted	Measured	Predicted	Measured	Predicted	Measured	Predicted	Measured	Predicted	Measured	Predicted	Measured
375	0.1678	0.168	17.3564	17.350	1974.8	1980	0.0489	0.049	17.8224	17.900	2009.3	2002
376	0.0852	0.085	17.0436	17.000	1986.7	1986	0.0351	0.035	17.8628	17.900	2038.4	2043
385	0.1727	0.172	16.7180	16.430	2018.1	2021	0.0350	0.035	17.9036	17.990	2032.6	2029
386	0.1766	0.174	16.6393	16.730	2027.6	2026	0.0290	0.029	17.6924	17.780	2058.9	2056
387	0.1296	0.129	16.1627	16.400	1978.0	1978	0.0350	0.035	17.6443	17.650	2010.8	2009
388	0.1432	0.144	16.4761	16.950	2044.4	2045	0.0439	0.044	17.7057	17.950	2046.0	2046
389	0.1021	0.092	16.4434	17.090	1985.8	1985	0.0310	0.031	17.1600	17.130	2022.3	2025
390	0.1746	0.174	15.9342	16.010	2035.1	2033	0.0280	0.028	18.1009	18.180	2054.6	2056
402	0.1802	0.180	17.2713	17.210	2047.0	2045	0.0371	0.037	17.7602	17.910	2052.1	2056
415	0.1502	0.150	17.0568	17.050	2057.0	2051	0.0380	0.038	17.9332	17.970	2045.6	2043
416	0.1822	0.185	17.0553	17.060	2046.8	2031	0.0329	0.033	18.2283	18.150	2054.7	2056
417	0.1463	0.148	17.0811	17.000	2039.6	2035	0.0451	0.045	18.1669	18.160	2046.2	2046
418	0.1665	0.164	15.3980	15.130	2024.0	2029	0.0420	0.042	17.7110	17.880	2039.3	2039
419	0.1599	0.158	16.3837	16.350	2042.9	2042	0.0410	0.041	18.0366	18.210	2028.8	2029
420	0.0653	0.065	17.6211	17.620	2025.8	2025	0.0331	0.033	18.0584	18.240	2032.0	2032
454	0.1305	0.134	17.0785	17.130	1927.3	1927	0.0450	0.045	17.9401	17.990	2051.1	2050
455	0.1497	0.149	17.8904	17.890	1946.3	1946	0.0581	0.058	18.1644	18.180	2038.9	2038
456	0.1702	0.170	17.4938	17.390	2058.2	2048	0.0350	0.035	17.6359	17.710	2031.5	2029
457	0.1513	0.154	15.0735	15.030	1999.5	2000	0.0350	0.035	16.2212	16.410	1999.7	2001
458	0.1148	0.113	14.5574	14.580	2027.8	2024	0.0250	0.025	15.7411	15.930	1988.6	1974
459	0.1045	0.103	16.9731	16.980	2003.0	2003	0.0330	0.033	17.6931	17.790	2027.9	2028
461	0.0405	0.040	17.2604	17.460	1966.2	1966	0.0269	0.027	17.9499	17.952	2061.6	2061
462	0.0920	0.091	16.9520	16.940	1971.1	1971	0.0322	0.032	17.9575	18.210	2066.0	2061
463	0.1142	0.113	16.8451	16.720	2027.9	2027	0.0359	0.036	17.7066	17.970	2042.6	2046
466	0.0984	0.097	17.1419	17.142	2013.2	2013	0.0421	0.042	17.7755	17.770	2022.2	2023
478	0.2031	0.206	17.9791	17.910	2013.6	2013	0.0310	0.031	17.6422	17.780	2036.3	2030
479	0.1337	0.132	16.9004	16.630	2056.2	2056	0.0280	0.028	18.0026	18.000	2053.7	2053
490	0.1517	0.150	17.3485	17.390	1949.3	1949	0.0380	0.038	17.8487	17.980	2062.7	2062

12, endpoint of oxygen side blowing operation; 13, endpoint of reduction period.

At the initial stage of the blowing process, although the bath temperature is relatively lower, the concentrations of C, Cr, Si and Mn in the molten steel all decrease; the oxidation reactions of Si and Mn with low initial contents quickly reach their respective dynamic equilibria and, the both basically no longer consume oxygen. Owing to adding high-carbon Fe–Cr, the Cr concentration increases to some extent. With progressing of the blowing process, the bath temperature fast rises. Relevantly, the oxidative loss of carbon is accelerated and its concentration significantly drops down, to 0.16 mass% when the bath temperature rising to the highest value at the moment of stopping the oxygen top blowing operation, then nearly keeping constant. Thereafter, the bath temperature is gradually falling down by adding of alloy agents, cooling materials and lime. Correspondingly, the oxidation reactions in the steel weaken. Adding high-carbon Fe–Cr increases the C and Cr concentrations. Simultaneously, the oxidation reaction of Cr is aggravated, but its concentration quickly decreases to the lowest value, then gradually approaching a stable state until cutting off oxygen supply by side blowing. In this period, the oxidation reactions of Si and Mn in the steel are not affected by the bath temperature and the oxidation extents of the other elements, basically maintaining their dynamic equilibria. It is necessary to point out that the dynamic equilibria of the oxidation reactions of Si and Mn are all the

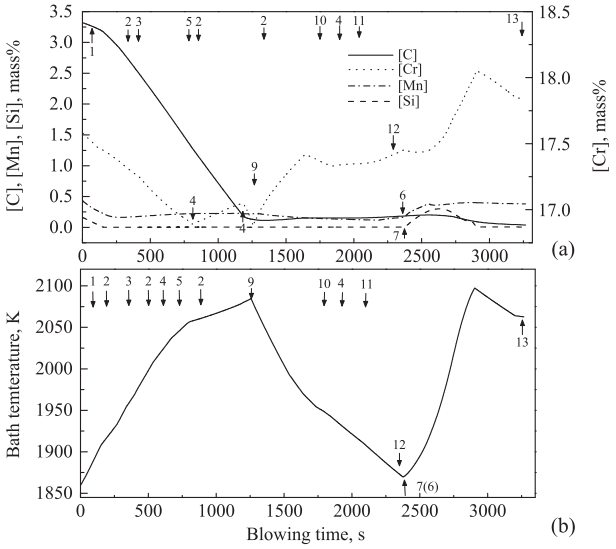

Fig. 1. Model predictions of concentrations of C, Cr, Si and Mn in molten steel (a) and bath temperature (b) during the whole AOD refining process at a higher initial carbon level (for heat 490).

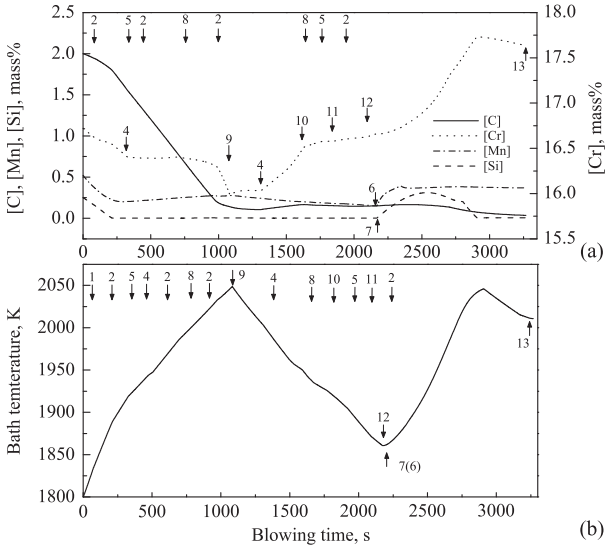

Fig. 2. Model predictions of concentrations of C, Cr, Si and Mn in molten steel and bath temperature during the whole AOD refining process at a lower initial carbon level (for heat 387).

results attained in competition in the case of all the possible reactions in the system simultaneously taking place.[14–16] With Si and Mn exiting (but still restricting) the competition of consuming oxygen, the oxidation reactions of C and Cr are intensified. In the reduction stage, adding Fe–Mn and Fe–Si leads to an increase in these contents. Mn rapidly attains a new equilibrium. At this time, the reduction of the oxide of Cr in the slag by Si increases the bath temperature again quickly. Additional oxidation of carbon also occurs after its slight concentration increasing. As a result of Cr_2O_3 reduction by Si, the content of Cr increases fast. The changes in the composition of the molten steel and bath temperature are not completely consistent with our previous investigation due to the discrepancies of the blowing operations and conditions from each other. But the basic patterns roughly are the same each other. The slag composition at the endpoint of the reduction period evaluated by the model is (mass%): 7.76 Cr_2O_3, 27.54 SiO_2, 5.88 MnO, 1.36 Al_2O_3, 2.53 FeO, 52.81 CaO, 2.08 MgO, well agreeing with the practice. For the other heats with a lower initial carbon content, the changing patterns of the composition of liquid steel and bath temperature during the whole refining process are basically the same as those for heat 490. As an example, the results for heat 387 with the initial carbon of 2.00 mass% are shown in **Fig. 2**.

5.3. Distribution Ratios of Blown Oxygen among Elements and Oxygen Supply Ratios of Oxides

The changes in the distribution ratios of blown oxygen among C, Cr, Si, and Mn dissolved in the molten steel and the oxygen supply ratios of the related oxides in the slag (for heat 385) are illustrated in **Figs. 3**(a) and 3(b), respectively.

The results are considered to be reasonable. In spite of low initial content of Si, at the initial blowing period with a relatively low bath temperature, the oxygen consumed by Si still is maximal; and x_{Si} slowly increases. After the content of Cr_2O_3 in the slag reaches 5 mass% (its solubility in the slag[30]), it evidently increases (x_{Cr} relevantly reducing), then gradually decreases, and approaches zero with the Si content quickly achieving a dynamic equilibrium value. As presented in Fig. 3(a), the maximum value of x_{Si} at this stage is 0.42. Since the initial concentration of Mn is also low with its lower affinity with oxygen, x_{Mn} is minimal and constantly decreasing, and also (but non-synchronously with x_{Si}) approaches zero. For this heat, the maximum value of x_{Mn} at this stage is only 0.12. At the relevant initial carbon concentration and bath temperature, x_C at the initial refining stage is about 0.30; x_{Cr} is approximately 0.27. After Si and Mn exiting the competition of consuming oxygen, oxygen is mainly distributed to C and Cr. As well, the bath temperature rapidly heightens due to the oxidation of elements and the post-combustion of CO. Correspondingly, the ratio of oxygen consumed by the carbon uninterruptedly increases to 0.70–0.80. Then, x_C stably increases with a sustained decrease in x_{Cr}, and reaches the maximum (0.90) at

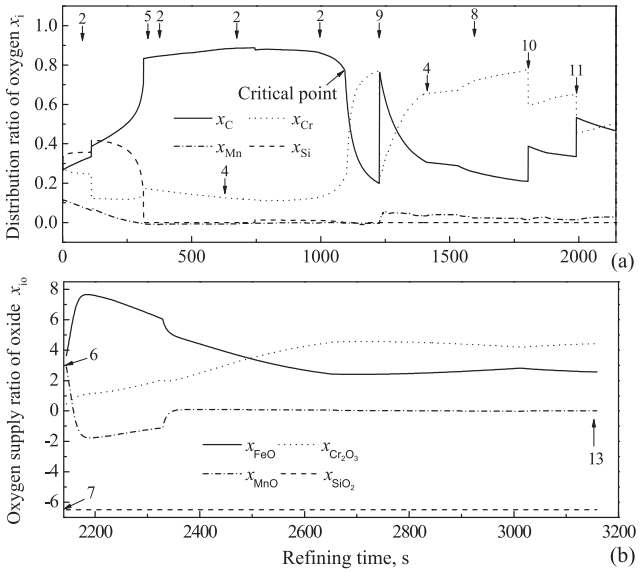

Fig. 3. Model predictions of distribution ratios of oxygen among elements during oxidation refining period (a) and oxygen supply ratios of oxides during Ar stirring and reduction refining (b) for heat 385.

the critical point of decarburization or the moment of terminating the oxygen top blowing. Adding the alloy agents makes the Si content in the steel slightly increase, thus the former equilibrium dramatically changes, resulting in $x_{Si}>0$.

The values of the oxygen distribution ratios for various heats are different each other, primarily dependent on the concrete conditions of the bath. Moreover, although Si and Mn no longer consume oxygen after x_{Si} and x_{Mn} are equal to zero, the both do not exit the oxidation-reduction reactions in the system, and still affect the distribution of oxygen between C and Cr. Under a certain condition, a small amount of MnO or SiO_2 in the slag may even be reduced, the relevant x_{Mn} or x_{Si} has a minus value, and the corresponding x_C is even larger than one (for heat 479).

After finishing the oxygen top blowing operation, the oxygen blown through the tuyeres is mainly consumed for the oxidative losses of C and Cr in the steel. But, x_C is uninterruptedly reducing and x_{Cr} is constantly increasing. It can be seen from Fig. 3(a) that x_{Cr} quickly increases near the critical point and then is larger than the appropriate x_C. The maximum value is about 0.80. It decreases to some extent or is transiently smaller than x_C only when changing the oxygen side blowing rate. At this time, x_{Si} may increase in a short time, and then the dynamic equilibrium of Si is continuously maintained, while Mn again demonstrates a demand for oxygen and takes part in the competition of consuming oxygen before the endpoint of the oxygen side blowing.

After oxygen blowing, Ar is continuously blown into the bath through the side tuyeres for agitating with a large amount of Fe–Si and Fe–Mn added to reduce Cr oxide in the slag. The content of SiO_2 in the slag rapidly increases with the reduction of the chromium oxide. As shown in Fig. 3(b), x_{SiO_2} presents a large minus value, while $x_{Cr_2O_3}$ has a smaller positive value. Cr_2O_3 in the slag still gives a certain contribution to decarburization in the case of its reduction by abundant Si.[21–23] As shown in Fig. 3(b), x_{FeO} approaches a considerable positive value, and even can always be larger than $x_{Cr_2O_3}$ at a certain condition (for heat 479). This indicates that FeO in the slag offers a larger amount of oxygen for the losses of Si and C. Except in the earlier stage of reduction, MnO in the slag basically does not supply oxygen.

It is necessary to point out that the values of the distribution ratios of oxygen and oxygen supply ratios of the oxides given are dependent not only on the Gibbs free energies of the reactions, but also on the composition and temperature of the bath. The latter are strongly related to many factors, such as the blowing conditions, the flow and mixing in the bath during the blowing process, the kinetics of the refining process, the heat and mass balances in the system, *etc*.

5.4. Decarburization Rate and Critical Carbon Concentration

Figure 4 gives the change in the total (combined blowing) decarburization rate (for heat 385). As blowing process proceeds with bath temperature rising, the decarburization rate gradually increases. Then, it attains a relatively stable value in a short time. Appropriately, the rate is directly affected by the oxygen flow rate. Moreover, adding the alloy agents and slag materials and scrap or crop ends can also influence the combined equilibrium at the reaction interface and x_C, thus changing the decarburization rate. After the carbon content of molten steel reduces to a low level and achieves the critical point value, the decarburization rate obeys dependently on the mass transfer of carbon in liquid steel. However, at this moment, the decarburization is still concerned with the oxygen flow rate, only its action is greatly weakened. In the Ar agitating stage after oxygen supply, the bubbles generated by Ar blown through the tuyeres have a diluting role to CO, the decarburization process is still proceeding. Si in the added ferrosilicon can make carbon activity rise. Its concentration at the interface further decrease to a lower level, and its deoxidation power increases to some extent. Thus, the decarburization rate also increases slightly. For this heat, the critical point of combined decarburization is (1096 s, 1.9239×10^{-3} mass%/s). For heats 462 and 479, the points are (1230 s, 2.7471×10^{-3} mass%/s), (1358 s, 5.5930×10^{-4} mass%/s), respectively.

Figure 4 also gives the changes in the decarburization rates of the top and, side blowing with the refining time for heat 385. At the combined blowing period, the decarburization rate resulted from side blowing is larger than that by top blowing. This is contrary to the result obtained in the previous investigation with a larger oxygen top blowing rate.[14–16] The contributions of the oxygen top blowing to the total decarburization under the present conditions are about 40–50%. When the initial carbon level is high, adding the oxygen top blowing operation to the traditional (simple side blowing) AOD refining process can remarkably intensify the decarburization, resulting in shortening the decarburization time.

With regard to the critical carbon concentration of decarburization, on the one hand, it is dependent upon the thermodynamic and kinetic considerations in the process and system. Further, it is also affected by many factors, such as the bath composition and temperature, the activities of components in the steel and slag, the partial pressure of CO, the blowing rates of oxygen and inert gas, the stirring and mixing state in the bath, the reaction interface, the geometry of the vessel, *etc.*[13] The results showed that under the present conditions, the critical carbon content for the overall decarburization refining process is in the range of (0.145–0.255) mass%. This is lower than that obtained in our previous investigation with an initial carbon content of 4.2 mass%.[14–16] Furthermore, the critical points of decarburization for top and side blowing are also different each

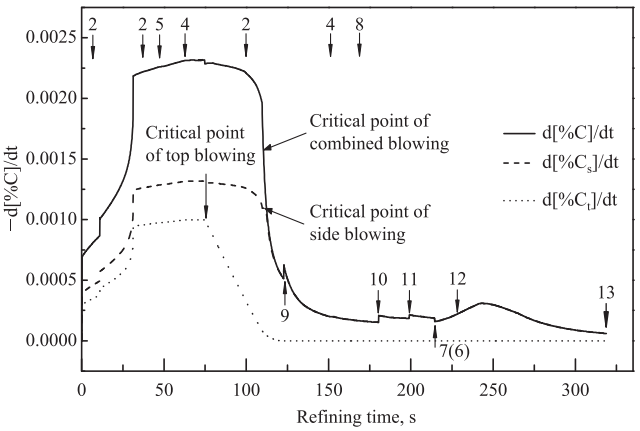

Fig. 4. Changes in decarburization rates of top, side, and combined blowing during the whole refining process with refining time for heat 385. Critical point of combined blowing: 1096 s, 1.9239×10^{-3} mass%/s.

other, without coinciding with that of the relevant combined blowing. Usually, the point for the top blowing earliest occurs, and that for the side blowing latest emerges. For the top and side blowing processes of heat 385, the appropriate critical carbon concentrations are 0.942 and 0.224 mass%. For heats 462 and 479, those are 1.895, 1.218 mass% and, 0.195, 0.145 mass%, respectively.

5.5. Effect of Initial Temperature of Molten Steel

Properly raising the starting blowing temperature would be beneficial to removing the carbon in the steel and enhancing the chromium recovery. However, the situations for various heats are different each other. The effect of the initial temperature of molten steel was examined. Varying the initial temperature with extent ±10 K, while keeping the other conditions constant, heat 385 was predicted as given in **Fig. 5**.

In the case of higher initial temperature (+10 K), at the reduction endpoint of this heat, the carbon content decreases from 0.035 to 0.034 mass%, and the chromium content increases from 17.90 to 17.92 mass%. The bath temperature is contrary slightly lower. With lower initial temperature (−10 K), the relevant carbon content increases to 0.036 mass%, while the chromium content decreases to 17.88 mass%. The bath temperature increases by 1 K. This suggests that suitably enhancing the initial temperature of molten steel is favorable to carbon removal and chromium recovery. As for the bath temperature at the reduction endpoint, it is also related to the addition amounts of Fe–Mn and Fe–Si, the Ar blowing rate and the concrete situations of the bath and others, besides the initial temperature. As presented in Fig. 5(c), the changes in the bath temperatures of the three cases before adding Fe–Si are all more stable, and after that, the temperature discrepancies among the three gradually lessens.

It should be said that the deviation of ±10 K is not significant. However, it is well known that the refining operations corresponding to different starting blowing temperatures, particularly the times and amounts of adding agents, the total refining time and others, must be different each other. The fixed operations of the original process, obviously, are no longer reasonable and cannot be used again for that with large deviation in initial temperature. Therefore, in the case of maintaining the other initial and boundary conditions constant, it is not suitable to take large deviation in the temperature. Otherwise, there is no comparability of the model predictions for different refining processes only with different initial temperatures. This is the main reason why the deviation of ±10 K has been chosen here. It is also necessary to point out that the model outputs in composition at the deviation are within analytical errors, although a changing tendency can be seen. The precision of the predictions by the new model is also much higher than that given in our preliminary investigation.[15)]

Generally, a lower carbon content and smaller chromium loss at the refining endpoint can be attained with a higher initial temperature of molten steel. As well, the amount of Cr_2O_3 needed to be reduced by Si in the reduction stage is smaller. Thus, the concentration of Si at the reduction endpoint is higher with a same addition of Fe–Si. As a result, it would be ensured in practical producing that the initial temperature of molten steel and starting blowing temperature are high enough to conduct successfully the refining process and to obtain a better refining result.

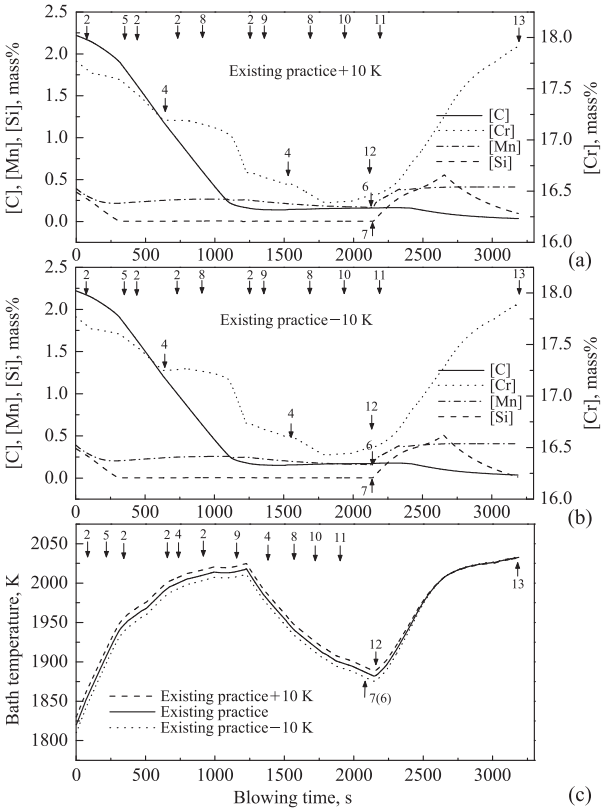

Fig. 5. Changes in contents of C, Cr, Si, and Mn in liquid steel at an initial temperature of original value +10 K (a) and −10 K (b) and bath temperature at the different initial temperatures (c) during the whole refining process of heat 385.

5.6. Influence of Gas Blowing Rates on the Decarburization Process

The gas flow rates influence the oxidation of the elements dissolved in the steel. And, these have much to do with optimizing of the ratio of oxygen to inert gas (N_2 or Ar). The model predictions clearly illustrate that the critical point always emerges before the endpoint of the main decarburization period in the blowing practice (Fig. 3). The surplus oxygen is almost all consumed for the loss of the chromium after the critical point. This suggests that in the practice, the main decarburization stage is too long. It may result in increasing the consumptions of reductants, slag materials, and oxygen, and in prolonging the refining time. It may also lower the working life of the lining. In fact, the supplied oxygen before the critical point is often inadequate in this practice. As far as the process optimization is concerned, this kind of blowing practice is evidently not reasonable.

Although the oxygen top blowing operation can obviously accelerate the decarburization of the earlier stage of refining, the results of physical modeling[17,19,20,29)] indicated that the existence of a gas top blowing jet is not advantageous to the liquid mixing in the bath. Under the conditions of simple side blowing, appropriately increasing the oxygen and nitrogen blowing rates in a certain range can cause a more optimal mixing effectiveness. That is favorable to intensifying the decarburization in the main decarburization period and to raising the rising rate of the bath temperature.[13)] Aiming at determining the effect of the gas blowing rates on the refining result along with optimizing

the oxygen top and side blowing rates, the refining processes with the assumed operating modes for heat 387 featuring a lower initial C content (2.0 mass%) were evaluated using the model. Here, the ratio of oxygen to inert gas is relevantly tried to optimize. The oxygen top blowing rate, the oxygen and nitrogen side blowing rates and the Ar flow rate in the reduction period were adjusted. The assumed operating modes are listed in **Table 5** with plotting in **Fig. 6** (for mode 1) and **Fig. 7** (for mode 4). The values focused on are listed in **Table 6**.

Comparative to those of the existing practice (Fig. 2), at the reduction endpoint of mode 1, the carbon content slightly decreases, the chromium content increases, and the bath temperature is essentially constant. With mode 2, the efficiency of carbon removal is better and the loss of Cr also somewhat lowers, with decreasing of the endpoint bath temperatures of the main decarburization and reduction periods respectively by about 33 and 3 K. This presents that at relatively low initial carbon levels, using the simple side blowing with a raised oxygen flow rate can also attain a better refining result. The endpoint carbon content of the reduction period for mode 3 further decreases, but the efficiency of preserving chromium decreases to some extent and the bath temperature obviously rises. In the case of mode 4, the carbon concentration is as low as 0.0149 mass% and the chromium content is as high as 17.902 mass% at the reduction endpoint, respectively decreasing and increasing by 0.021 and 0.26 mass%. Simultaneously, the endpoint bath temperatures at the main decarburization and reduction periods decrease by about 17 and 2 K, respectively. The composite refining result is much superior to that in the existing practice. This is resulted from improving the blowing operation. The improvement involves reducing the oxygen top blowing rate contrary with increasing the oxygen and nitrogen side blowing rates in the main decarburization period, decreasing the oxygen side blowing rates along with increasing the nitrogen blowing rates in the dynamic decarburization periods to lower the relevant ratios of oxygen to nitrogen, and raising the Ar flow rate in the reduction period.

Thus, suitably adjusting the oxygen and nitrogen blowing rates with reducing the ratios of oxygen to nitrogen of the blowing periods, can evidently improve the refining effectiveness. For the combined refining process, decreasing the oxygen top blowing rate and increasing the oxygen and nitrogen side blowing rates depending on the initial carbon content and temperature of molten steel can raise the oxygen utilization efficiencies, resulting in acceleration of the decarburization. After the critical point, decreasing the oxygen side blowing rate and enhancing the nitrogen flow rate to lower the ratio of oxygen to nitrogen can more effectively dilute CO by N_2, further promoting the decarburization. Appropriately enlarging the Ar flow rate in the reduction period is conducible to deep decarburizing and to further reducing of the Cr_2O_3 in the slag.

6. Conclusions

(1) The mathematical model proposed can well reflect the actualities in the combined side and top blowing AOD process of stainless steel. It can accurately calculate the changes in the concentrations of C, Cr, Si, and Mn in the steel and bath temperature with the refining time during the whole process.

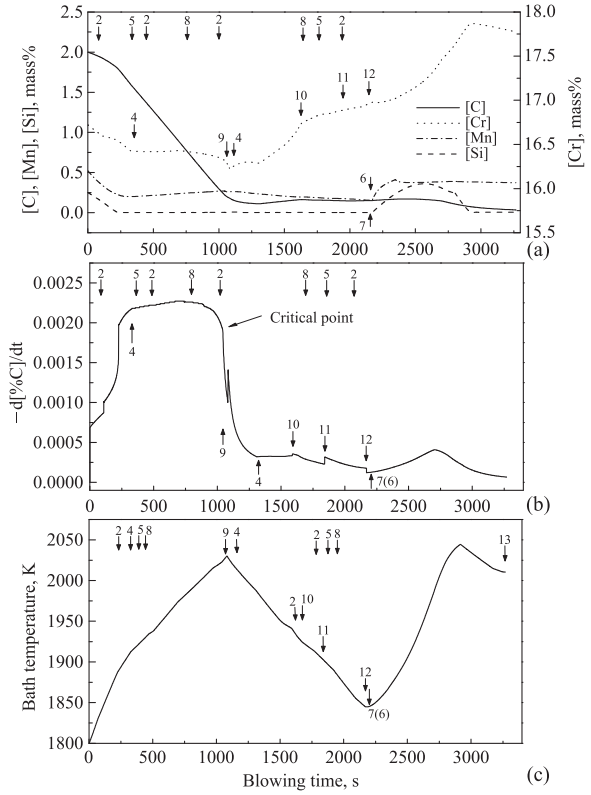

Fig. 6. Changes in composition of liquid steel (a), decarburization rate (b) and bath temperature (c) with refining time for heat 387 at operating mode 1.

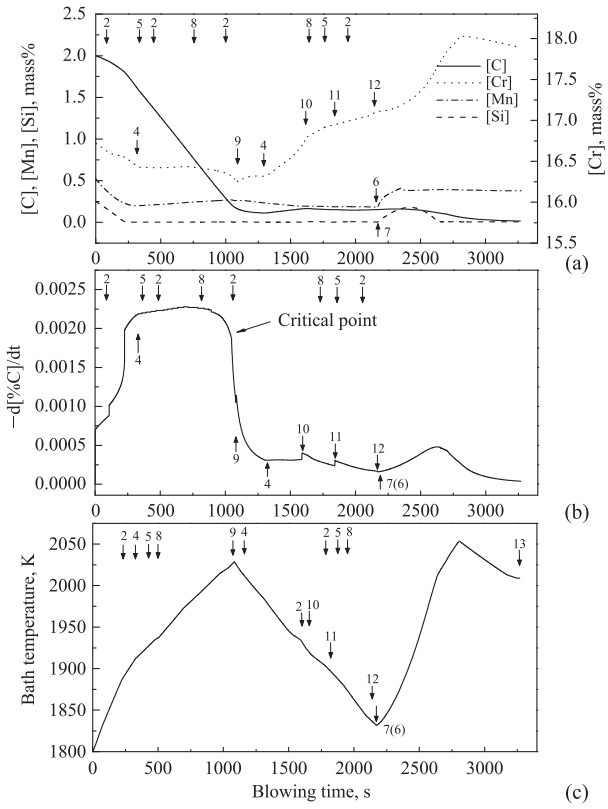

Fig. 7. Changes in composition of liquid steel (a), decarburization rate (b) and bath temperature (c) with refining time for heat 387 at operating mode 4.

(2) The Gibbs free energies of the oxidation and reduction reactions can be utilized to characterize well the competitive oxidation among the elements in the steel and the

Table 5. Existing practice and assumed blowing modes for heat 387 (unit of the gas flow rate: Nm^3/min).

Heat No.	Blowing operating mode.	O_2 top	O_2 side blowing				N_2 side blowing				Ar side blowing
		Main decarburization period	Main decarburization period	Dynamic period 1	Dynamic period 2	Dynamic period 3	Main decarburization period	Dynamic period 1	Dynamic period 2	Dynamic period 3	Reduction period
387	Existing	110	110	60	40	30	30	60	80	110	80
	1	130	110	65	30	25	30	70	80	115	80
	2	0	200	50	35	25	30	60	80	110	90
	3	90	125	70	50	35	40	65	85	115	80
	4	100	130	60	25	18	45	70	95	125	120
	5	130	110	65	30	25	30	70	80	115	106.7
	6	115	105	65	35	25	30	65	80	115	90
	7	110	130	65	35	25	40	70	85	120	80
	8	110	130	65	35	25	40	70	85	120	90
	9	110	120	60	30	20	40	75	90	120	100
	10	110	120	60	30	20	40	75	95	130	100

Table 6. Refining results predicted by the model at different blowing modes for heat 387.

Heat No.	Blowing mode	[C], mass%		[Cr], mass%		Bath temperature *T*, K	
		End of main decarization period	End of reduction period	End of main decarization period	End of reduction period	End of main decarization period	End of reduction period
387	Existing	0.1296	0.0350	16.1627	17.6443	1978.0	2010.8
	1	0.1302	0.0343	16.4073	17.7830	1965.8	2010.5
	2	0.1499	0.0307	16.3644	17.7125	1944.6	1997.7
	3	0.1186	0.0272	16.1580	17.6122	1981.7	2018.8
	4	0.1321	0.0149	16.4485	17.9020	1960.8	2008.9
	5	0.1302	0.0178	16.4073	17.8533	1965.8	2009.8
	6	0.1175	0.0234	16.1579	17.7076	1982.9	2014.1
	7	0.1144	0.0306	16.2089	17.6865	1982.3	2017.6
	8	0.1144	0.0237	16.2089	17.7303	1982.3	2015.9
	9	0.1377	0.0241	16.5531	17.9079	1952.6	2005.4
	10	0.1377	0.0244	16.5531	17.9050	1952.6	2006.6

competitive reduction of the oxides in the slag, as well to determine reasonably the relevant oxygen distribution ratios of the elements and oxygen supply ratios of the oxides.

(3) The critical carbon concentrations of decarburization for the top, side and combined blowing of 304-grade steel in this work are in the ranges of 0.895 to 0.942, 0.078 to 0.224, 0.144 to 0.255 mass%, respectively.

(4) The starting blowing temperature should be high enough to progress smoothly the refining process and to achieve a good refining effectiveness.

(5) Suitably determining the oxygen top and side blowing rates with the oxygen ratios to nitrogen is important for optimizing the blowing technology.

(6) Relative to the existing practice, properly decreasing the oxygen top blowing rate and increasing the oxygen and nitrogen flow rates from side tuyeres can intensify the decarburization in the main decarburization period. After the critical point, suitably reducing the oxygen side blowing rate and enhancing the nitrogen flow rate can further promote the decarburization. Raising the Ar flow rate in the reduction period is conducible to deep decarburizing and to further reducing the Cr_2O_3 in the slag.

(7) The model can provide a reliable basis and useful information for determining and optimizing the technology of the combined blowing AOD process of stainless steel, and controlling the process in real time and on-line.

Acknowledgement

The authors gratefully acknowledge the combined support of The National Natural Science Foundation of China and Shanghai Bao Steel (Group) Co. Ltd. (Grant No. 50374047).

REFERENCES

1) W.-H. Ray and J. Szekely: Process Optimization with Applications in Metallurgy and Chemical Engineering, John Wiley & Sons, Interscience, New York, (1971), 310.
2) S. Asai and J. Szekely: *Metall. Trans.*, **5** (1974), No. 3, 651.
3) J. Szekely and S. Asai: *Metall. Trans.*, **5** (1974), No. 7, 1573.
4) R. J. Fruehan: *Ironmaking Steelmaking*, **3** (1976), No. 3, 153.
5) T. Deb Roy and D. G. C. Robertson: *Ironmaking Steelmaking*, **5** (1978), No. 5, 198.
6) T. Deb Roy and D. G. C. Robertson: *Ironmaking Steelmaking*, **5** (1978), No. 5, 207.
7) T. Ohno and T. Nishda: *Tetsu-to-Hagané*, **63** (1977), No. 13, 2094.
8) T. Tohge, Y. Fujita and T. Watanabe: Proc. 4th Process Technology Conf., ISS, Warrendale, PA, USA, (1984), 129.
9) J. Reichel and J. Szekely: *Iron Steelmaker*, (1995), No. 5, 41.
10) D. A. Lewis, D. E. Pauley, C. E. Rea, M. E. Shupay and J. D. Nauman: Proc. Annual Convention of 1998 AISE (CD edition), AISE, Warrendale, PA, (1998).
11) M. Gornerup and P. Sjoberg: *Ironmaking Steelmaking*, **26** (1999), No. 1, 58.
12) J.-H. Wei and D.-P. Zhu: *Metall. Mater. Trans. B*, **33** (2002), No. 1, 111.
13) J.-H. Wei and D.-P. Zhu: *Metall. Mater. Trans. B*, **33** (2002), No. 1, 121.
14) H.-L. Zhu, J.-H. Wei, G.-M. Shi, J.-H. Shu, Q.-Y. Jiang and H.-B. Chi: *Steel Res. Int.*, **78** (2007), No. 4, 305.
15) G.-M. Shi, J.-H. Wei, H.-L. Zhu, J.-H. Shu, Q.-Y. Jiang and H.-B. Chi: *Steel Res. Int.*, **78** (2007), No. 4, 311.
16) J.-H. Shu: M. D. Thesis, Shanghai University, (2004).
17) H.-L. Zhu: Ph. D. Thesis, Shanghai University, (2006).
18) Y. Cao: M. D. Thesis, Shanghai University, (2005).
19) J.-H. Wei, H.-L. Zhu, H.-B. Chi and H.-J. Wang: *ISIJ Int.*, **50** (2010), No. 1, 17.
20) H.-J. Wang: M. D. Thesis, Shanghai University, (2005).
21) C.-H. Wei (J.-H. Wei) and A. Mitchell: Proc. 3rd Process Technology Conf., Vol. 3, AIME, AISE, Warrendale, PA, USA, (1982) 232.
22) J.-H. Wei and A. Mitchell: *Acta Metall. Sin.*, **20** (1984), No. 5, B261.
23) J.-H. Wei and A. Mitchell: *Chin. J. Met. Sci. Technol.*, **2** (1986), No. 1, 11.
24) J.-H. Wei and A. Mitchell: *Acta Metall. Sin.*, **23** (1987), No. 3, B126.
25) J.-H. Wei: *Chin. J. Met. Sci. Technol.*, **5** (1989), No. 4, 235.
26) J.-H. Wei and H.-Y. Zuo: *Steel Res. Int.*, **78** (2007), No. 12, 863.
27) J.-F. Yao, C. Mei, H.-J. Ren, J. Hu and J.-H. Jiang: *Chin. J. Nonferrous Met.*, **10** (2000), No. 4, 546.
28) F. Oeters: Metallurgy of Steelmaking, Verlag Stahleisen mbH, Düsseldorf, Germany, (1994).
29) J.-H. Wei, H.-L. Zhu, H.-B. Chi and H.-J. Wang: *ISIJ Int.*, **50** (2010), No. 1, 26.
30) E. T. Turkdongan: Physicochemical Properties of Molten Slag and Glasses, Metals Society, London, (1983), 422.